
Proceedings Paper:
Alanazi, N., Kolawole, J.T., Buswell, R. et al. (1 more author) (2023) The Theory of Critical Distances to perform the static assessment of 3D-printed concrete weakened by manufacturing defects and cracks. In: Procedia Structural Integrity. European Conference on Fracture 2022 (ECF23), 27 Jun - 01 Jul 2022, Funchal, Portugal. Elsevier , pp. 336-342.

https://doi.org/10.1016/j.prostr.2022.12.041

Available online at www.sciencedirect.com

ScienceDirect

Procedia Structural Integrity 42 (2022) 336–342

Structural Integrity Procedia

www.elsevier.com/locate/procedia

23 European Conference on Fracture - ECF23

The Theory of Critical Distances to perform the static assessment of 3D-printed concrete weakened by manufacturing defects and cracks

N. Alanazi[a,b], J. T. Kolawole[c], R. Buswell[c], L. Susmel[b,*]

[a]*Department of Civil Engineering, College of Engineering, University of Hail, Hail, 81411, Kingdom of Saudi Arabia*
[b]*Department of Civil and Structural Engineering, The University of Sheffield, Mappin Street, Sheffield, S1 3JD, United Kingdom*
[c]*School of Architecture Building and Civil Engineering, Loughborough University, Loughborough, LE11 3TU, United Kingdom*

Abstract

The Theory of Critical Distances groups together a number of approaches postulating that, in cracked/notched materials subjected to static loading, breakage takes place as soon as a critical length-dependent effective stress exceeds the material tensile strength. The characteristic length used by the Theory of Critical Distances is a material property that can directly be estimated from the ultimate tensile strength and the plane strain fracture toughness. In the present investigation, based on a large number of bespoke experimental results, it is demonstrated that the Theory of Critical Distances is successful also in quantifying the detrimental effect of cracks and manufacturing defects in 3D-printed concrete subjected to Mode I static loading.

Keywords: Type your keywords here, separated by semicolons ;

1. Introduction

There has been a significant increase in the number of cementitious based, large-scale, additive manufacturing processes under development internationally over the last 10 years (Ma et al., 2022). These methods utilise precise placement of material under computer control to additively build a component or structure, removing the requirement

* Corresponding author. Tel.: +0-000-000-0000 ; fax: +0-000-000-0000 .
E-mail address: l.susmel@sheffield.ac.uk

10.1016/j.prostr.2022.12.041

and substantial cost of conventional moulds. This in turn releases the designer from the millennia-old constraint of minimizing the number of component variants to maximize the number of elements cast from each mould.

A further advantage of the most sophisticated current technology is that complex geometries such as double-curved surfaces can be created at the same cost and speed as the simple flat panel geometries, usually created with traditional casting methods. Furthermore, the removal of moulds (or shuttering) also makes possible the automated, in-situ placement of the material, so that site based operations such as structural walls and columns can also be constructed using layer-based techniques. The technology thus lends itself to on/off-site, factory-based, high-value component manufacture and to on-site automated construction. Both applications have the potential for streamlining work flow on site through just-in-time manufacturing, introducing more variability in the design of structures, reducing material usage and waste, as well as removing operatives from the need to directly handle harmful materials in dangerous environments.

While this exciting technology has a great potential yet to be exploited in full, a main barrier against large-scale use of modern 3D printing techniques in additively manufactured concrete is the lack of specific structural analysis tools. In this setting, this paper reports on an attempt of extending the use of the Theory of Critical Distances (Taylor, 2007) to the static assessment of additively manufactured concrete containing cracks and manufacturing defects.

Nomenclature

a	crack length
a_0	theoretical crack length delimiting the long-crack regime
F	shape factor
K_c	fracture toughness
K_I	mode I Stress Intensity Factor (SIF)
K_{Ic}	plane strain fracture toughness
L	critical distance
Oxy	system of coordinates
r, θ	polar coordinates
θ_p	angle between 3D-printing filaments and specimen's longitudinal axis
σ_{eff}	effective stress estimated according to the Theory of Critical Distances
σ_{FS}	plain material flexural strength
σ_g	nominal gross stress
σ_t	tensile strength
σ_{UTS}	ultimate tensile strength
σ_{th}	nominal gross stress resulting in the static breakage of cracked materials

2. The short crack regime problem

In the Linear-Elastic Fracture Mechanics (LEFM) discipline, the Stress Intensity Factor (SIF) is used to describe in a concise, effective way the entire linear-elastic stress field in the vicinity of the tip of the crack being analysed. The SIF under Mode I loading can be quantified according to this well-known definition (Anderson, 1995):

$$K_I = F\sigma_g\sqrt{\pi \cdot a} \tag{1}$$

where a is the crack length, σ_g is the nominal gross stress, and F is the so-called shape factor which depends on the geometrical/loading configuration characterising the specific case being considered. LEFM assumes that, in a cracked material subjected to Mode I static loading, failure takes place as soon as K_I equals the material fracture toughness, K_c. Based on this assumption, Eq. (1) can easily be rewritten for the incipient failure condition case (i.e., K_I=K_c). Accordingly, that the magnitude of the nominal gross threshold stress, σ_{th}, resulting in static breakage takes on the following value:

$$\sigma_{th} = \frac{K_c}{\sqrt{\pi(F^2 \cdot a)}} \tag{2}$$

The threshold condition estimated according to Eq. (2) can then be plotted in a Kitagawa-Takashi (1976) like (log-log) diagram (Fig. 1) plotting σ_{th} against an equivalent crack length calculated as F^2a (Usami, 1985). The key feature of this simple way of modelling fracture is that experimental results obtained via cracked specimens characterised by different values of F can all be brought back to the reference case of a central through-thickness crack in an infinite plate loaded in tension. For this reference case, the shape factor, F, is invariably equal to unity. According to the log-log diagram seen in Fig. 1, Eq. (2) states that σ_{th} increases as the equivalent crack length decreases, eventually becoming larger than the material tensile strength, σ_{UTS}. Since a material cannot be characterised by a strength that is larger than its intrinsic ultimate tensile strength, the schematisation of Fig. 1 suggests that the LEFM concepts can be used to model the mechanical behaviour of cracked materials as long as the equivalent crack length is larger than a_0, that is:

$$F^2 \cdot a \geq a_0 = \frac{1}{\pi}\left(\frac{K_c}{\sigma_{UTS}}\right)^2 \tag{3}$$

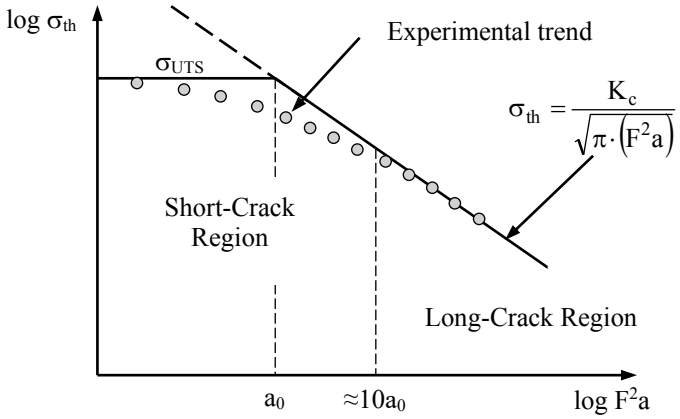

Fig. 1. Kitagawa-Takahashi diagram.

In this setting, as schematically shown in Fig. 1, much experimental evidence demonstrates that there exists a gradual transition from the short- to the long-crack regime (Usami et al., 1986). Thus, LEFM returns accurate estimates solely when the equivalent crack length is larger than about $10a_0$ (Taylor, 2007). The considerations reported above should make it evident that attention should always be paid not to use LEFM out of its range of validity; otherwise, the estimates of strength would be non-conservative. As it will be discussed in the next section, according to Taylor (2007), these problems can all be overcome in a very simple, effective way by modelling the fracture problem through the Theory of Critical Distances (TCD).

3. The short crack regime problem

The TCD assumes that static breakage takes place when a material critical length-related effective stress, σ_{eff}, becomes larger than σ_{UTS}. Based on this postulate, the incipient failure condition under Mode I static loading can then be formalised as follows:

$$\sigma_{eff} = \sigma_{UTS} \tag{4}$$

As per the state-of-the-art knowledge, σ_{eff} can be calculated according to either the Point, Line, Area, or Volume Methods (Taylor, 1999; Susmel & Taylor, 2008a; Susmel & Taylor, 2008b). Since the use of these different formalisations of the TCD results in similar estimates (Taylor, 2007), in what follows we will use the TCD solely in its simplest forms, i.e. the Point Method (PM) and Line Method (LM). According to the PM and LM then, σ_{eff} takes on the following values, respectively (Taylor, 2007):

$$\sigma_{eff} = \sigma_y(\theta = 0, r = L/2) \tag{5}$$

$$\sigma_{eff} = \frac{1}{2L}\int_0^{2L} \sigma_y(\theta = 0, r)dr \tag{6}$$

The meaning of the symbols being used is explained in Fig. 2a. In definitions (5) and (6), critical distance L is a material property that is estimated from the plane strain fracture toughness, K_{Ic}, and the ultimate tensile strength, σ_{UTS}, via the following well-known relationship (Whitney & Nuismer, 1974; Taylor, 2007):

$$L = \frac{1}{\pi}\left(\frac{K_{Ic}}{\sigma_{UTS}}\right)^2 \tag{7}$$

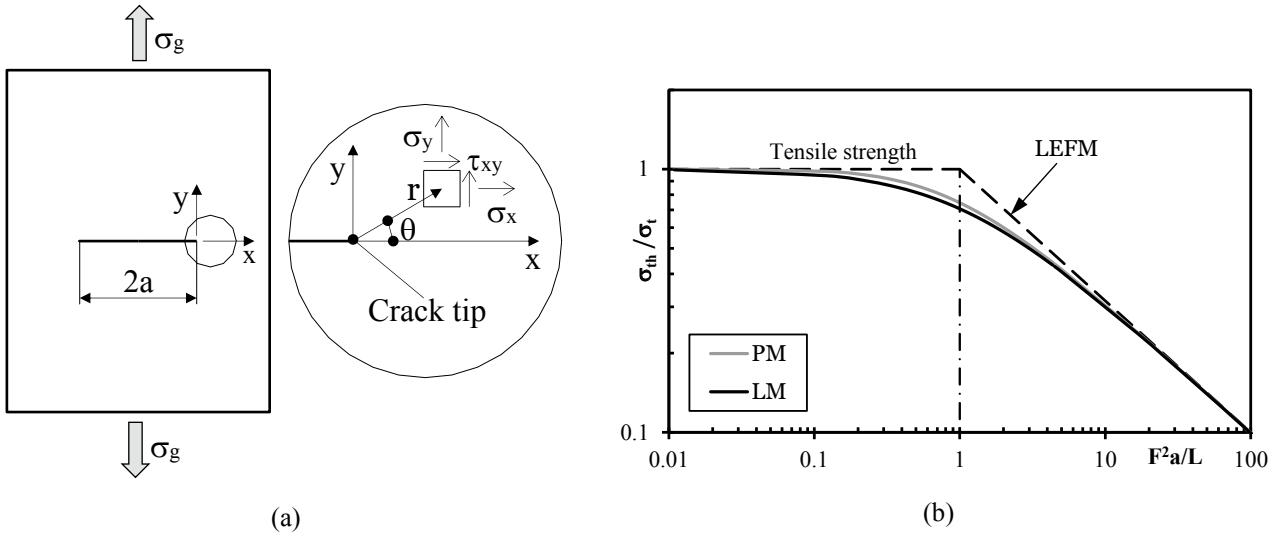

Fig. 2. (a) uniaxially loaded plate containing a central through-thickness crack; (b) normalised Kitagawa-Takahashi diagram and transition from the short- to the long-crack region modelled according to the PM and LM.

To use the PM and the AM to model the transition from the short- to the long-crack regime, consider a infinite plate containing a central through-thickness crack of semi-length a (Fig. 2a). This plate is assumed to be loaded in tension. By taking advantage of the classic analytical solution due to Westergaard (1939), the linear-elastic stress along the crack bisector (i.e., θ=0 in Fig. 2a) can be expressed as:

$$\sigma_y(\theta = 0, r) = \frac{\sigma_g}{\sqrt{1-\left(\frac{a}{a+r}\right)^2}} \tag{8}$$

If stress σ_y is calculated through Eq. (8) at a distance r from the crack tip equal to L/2 and the failure condition is expressed according to Eq. (4), the PM can directly be re-written to model the transition from the short- to the long-crack regime as (Taylor, 1999):

$$\sigma_{th} = \sigma_{UTS}\sqrt{1-\left(\frac{a}{a+L/2}\right)^2} \tag{9}$$

Following a similar strategy, the LM effective stress can directly be calculated as:

$$\sigma_{eff} = \frac{1}{2L}\int_0^{2L}\frac{\sigma_g}{\sqrt{1-\left(\frac{a}{a+r}\right)^2}}dr = \sigma_g\sqrt{\frac{a+L}{L}} \tag{10}$$

so that, according to failure condition (4), the transition from the short- to the long-crack regime can be modelled via the following simple relationship (Taylor, 1999):

$$\sigma_{th} = \sigma_{UTS}\sqrt{\frac{L}{a+L}} \tag{11}$$

The normalised Kitagawa-Takashi diagram seen in Fig. 2b makes it evident that the PM - expressed according to Eq. (9) - as well as the LM - formalised via Eq. (11) - are successful in linking the plain material static strength (on the left-hand side) with the cracked plate nominal strength estimated according to LEFM (on the right-hand side). While the estimates obtained from the two methods are very close to each other, in the transition region, the PM is seen to be slightly less conservative than the LM (see Fig. 2b).

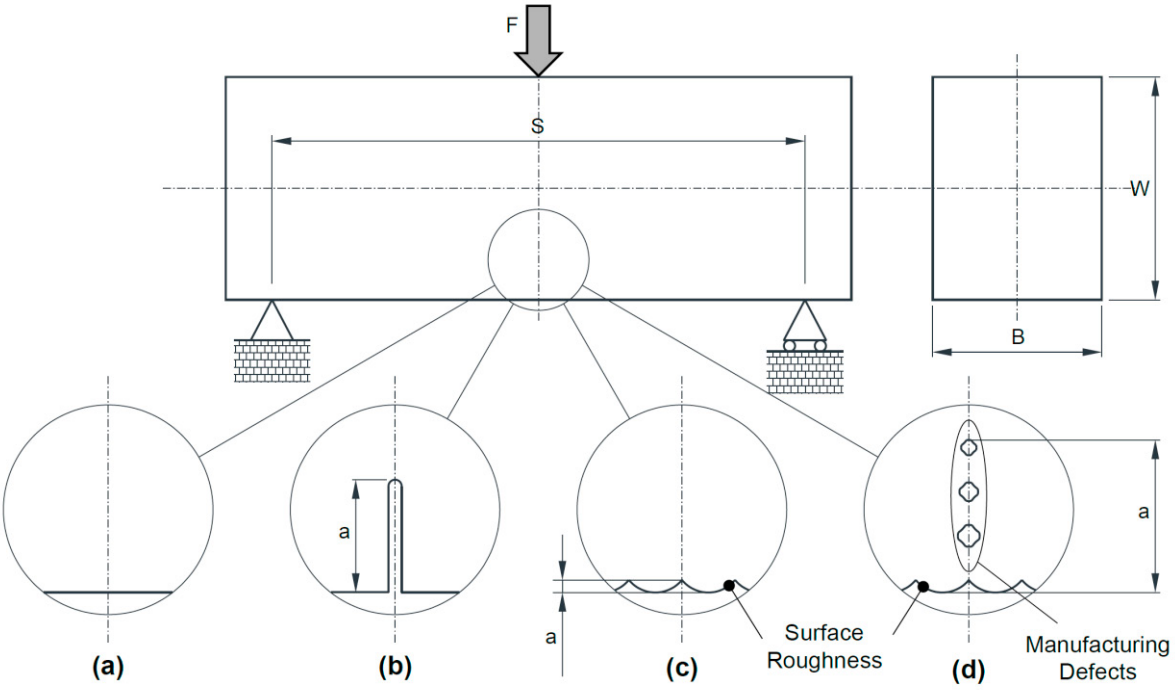

Fig. 3. 3D-printed specimens tested under three-point bending: plain specimen (a); specimen containing a saw-cut crack-like sharp notch (b); specimen weakened by surface roughness (c); specimen weakened by manufacturing defects (d).

4. Manufacturing of the 3D-printed concrete specimens

The specimens being tested were manufactured using the following ingredients: 52.5N CEM I Portland Cement, fly ash, silica fume, sand, water, polycarboxylate ester-based superplasticiser, and amino tris (methylene phosphonic

acid) based retarder (Lee et al., 2012a; Lee et al., 2012b). The parent material was 3D-printed using an ABB IRR 6640 6-axis robot. The concrete was extruded at a printing rate of 200, 225, and 250 mm/s by using a nozzle having diameter equal to 10 mm. During manufacturing, the layer height was set equal to 6 mm and the pump flow rate to 0.72 L/min. As soon as they were additively-manufactured, the slabs were covered for 24 hours and cured in water for 28 days. Print speeds of 225 and 250 mm/s were used to introduce manufacturing defects in the material due to volume mismatch. After post-manufacturing curing, the concrete slabs were saw-cut to make rectangular beams with width, W, in the range 44-53 mm and thickness, B, in the range 34-56 mm (Fig. 3). The rectangular section beams used to make the specimens were cut so that the printing direction was either parallel, θ_p=0°, or perpendicular, θ_p=90°, to the specimen longitudinal axis.

The specimens were tested under three-point bending (Fig. 3) up to complete breakage by setting the displacement rate equal to 33.3 N/sec. The span, S, between the lower rollers was set equal to either 60 mm, 80 mm, or 100 mm.

Other than the plain (i.e., un-notched) samples (Fig. 3a), three other different configurations were considered. These different configurations are described in what follows.

The specimens containing the crack-like sharp notches with depth a varying in the range 2-27 mm were fabricated using a circular tip blade having thickness equal to 2.6 mm (Fig. 3b).

A number of specific experimental results were generated to investigate the detrimental effect of the surface roughness resulting from the deposition filaments (Fig. 3c). For these specimens, the valleys characterising the surface texture were modelled as cracks. The depth, a, of these equivalent cracks was defined as the maximum valley depth below the filament peaks in the vicinity of the failure location. This simple geometrical definition for the depth of the equivalent cracks resulted in values of length a varying from 1.2 mm up to 3.5 mm.

A final batch of specimens was manufactured so that 3D-printing-induced flaws were introduced mainly on the side undergoing tensile stress during testing (Fig. 3d). For a given vertical cross section, the defects were assumed to be interlinked, resulting in an equivalent crack having length, a, defined as shown in Fig. 3d.

The complete description of the experimental results generated according to the above experimental protocol can be found in a recent article by Alanazi et al. (2022).

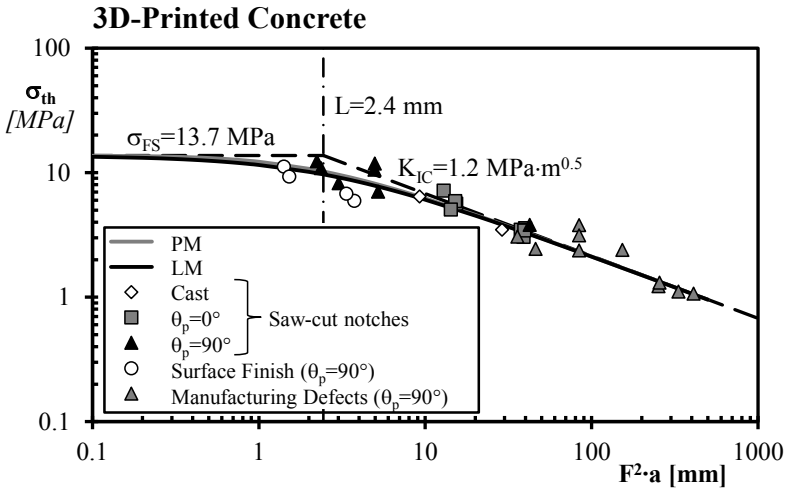

Fig. 4. (a) uniaxially loaded plate containing a central through-thickness crack; (b) normalised Kitagawa-Takahashi diagram and transition from the short- to the long-crack region modelled according to the PM and LM.

5. Accuracy of the TCD used in the form of the PM and LM

All the tested specimens were modelled using Finite Element (FE) code ANSYS® to determine the relevant linear-elastic stress fields. The samples were all schematised as single edge notched bend (SE(B)) beams where the notch tip

radius was set invariably equal to zero. Any individual FE model was built using the actual geometrical dimensions, with the crack length, a, for the various cases being defined as discussed in the previous section (see Fig. 3). The stress analysis was performed using bi-dimensional elements with thickness PLANE183. The mesh density was gradually increased in the vicinity of the crack tip in order to reach convergence in the determination of the stress intensity factor. The linear-elastic stress fields estimated from these FE models were then used to determine not only the stress intensity factors, but also the shape factors according to the standard procedure recommended by Anderson (1995).

Based on the experimental results being generated, the plain material flexural strength, σ_{FS}, and the plane strain fracture toughness, K_{Ic}, were estimated to be equal to 13.7 MPa and to 1.2 MPa·m$^{1/2}$, respectively. Having determined σ_{FS} and K_{Ic} for the 3D-printed concrete under investigation, Eq. (1) was used to estimate the critical distance value – where σ_{UTS} was directly replaced with σ_{FS}. This simple calculation returned a value for critical distance L of 2.4 mm.

These material constants together with the experimental results being generated were then used to build the Kitagawa–Takahashi diagram reported in Fig. 4. This chart summarises the overall accuracy of the TCD used in the form of the PM, Eq. (4), and LM, Eq. (5). The diagram of Fig. 4 makes it evident that the use of the TCD resulted in a remarkable level of accuracy, with this holding true independently of the type of local stress raiser being analysed.

6. Conclusions

- With 3D-printed concrete as well, LEFM is recommended to be used in the presence of cracks/defects having equivalent length $\alpha^2 a$ larger than 10L - where critical distance L is calculated via Eq. (7).
- The TCD is seen to be successful in modelling the transition from the short- to the long-crack regime under Mode I static loading in 3D-printed concrete containing cracks and manufacturing defects.

Acknowledgements

Support for this research work from the Engineering and Physical Sciences Research Council (EPSRC, UK) through the award of grants EP/S019650/1 and EP/S019618/1 is gratefully acknowledged. Nasser A. Alanazi is grateful to the University of Hail, Saudi Arabia, for sponsoring his PhD studentship.

References

Alanazi, N., Kolawole, J.T., Buswell, R., Susmel, L., 2022. The Theory of Critical Distances to assess the effect of cracks/manufacturing defects on the static strength of 3D-printed concrete. Engineering Fracture Mechanics 269, 108563.

Anderson, T. L., 1995. Fracture mechanics: Fundamentals and applications. Boca Raton, CRC Press.

Kitagawa, H., Takahashi, S., 1976. Application of fracture mechanics to very small cracks or the cracks in the early stage. Second International Conference on Mechanical Behaviour of Materials, ASM, pp. 627-630.

Le, T.T., Austin, S.A., Lim, S., Buswell, R.A., Law, R., Gibb, A.G.F., Thorpe, T., 2012a. Hardened properties of high-performance printing concrete. Cement and Concrete Research 42, 558-566.

Le, T.T., Austin, S.A., Lim, S., Buswell, R.A., Gibb, A.G.F., Thorpe, T., 2012b. Mix design and fresh properties for high-performance printing concrete. Materials and Structures 45, 1221–1232.

Ma, G., Buswell, R., Leal da Silva, W.L., Wang, L., Xu, J., Jones, S.Z, 2022. Technology readiness: A global snapshot of 3D concrete printing and the frontiers for development. Cement and Concrete Research 156, 106774.

Susmel, L., Taylor, D., 2008a. The theory of critical distances to predict static strength of notched brittle components subjected to mixed-mode loading. Engineering Fracture Mechanics 75, 534-550.

Susmel, L., Taylor, D., 2008b. On the use of the Theory of Critical Distances to predict static failures in ductile metallic materials containing different geometrical features. Engineering Fracture Mechanics 75, 4410-4421.

Taylor, D., 1999. Geometrical effects in fatigue: a unifying theoretical model. International Journal of Fatigue 21, 413-420.

Taylor, D., 2007. *The Theory of Critical Distances: A New Perspective in Fracture Mechanics*. Elsevier Science, Oxford, UK.

Usami, S., 1985. Short crack fatigue properties and component life estimation, in *"Current Research on Fatigue Cracks - Current Japanese Materials Research Series"*. In Tanaka, Jono, M., Komai, K. (Ed.). The Society of Materials Science, Vol. 1, Kyoto, Japan, pp. 119–147.

Usami, S., Kimoto, H., Takahashi, I., Shida, S., 1986. Strength of ceramic materials containing small flaws. Engineering Fracture Mechanics 23, 745-761.

Westergaard, H. M., 1939. Bearing pressures and cracks. Journal of Applied Mechanics A 61, 49-53.

Whitney, J.M., Nuismer, R.J., 1974. Stress Fracture Criteria for Laminated Composites Containing Stress Concentrations. Journal of Composite Materials 8, 253-65.